Journal of Visualization, Vol. 2, No. 1 (1999) 59-71

Visualizing Strake and Wing Vortices in Supersonic Flow by a Thermographic Technique

Zuppardi, G.* and Valenza, F.*

*Università di Napoli "Federico II", Dipartimento di Scienza ed Ingegneria dello Spazio "Luigi G. Napolitano", P.le V. Tecchio 80, 80125 Napoli, Italy.

Received 24 January 1999.
Revised 1 June 1999.

***Abstract*:** The Unsteady Computerized Thermographic Technique (UCTT) provides patterns of the Stanton number on a body surface. These patterns are the imprints of the flow field. The UCTT already proved to be a powerful, not intrusive diagnostic tool both for the visualization and the strength evaluation of vortical structures on the lee-side surface of delta wing models. The patterns are obtained by processing, by an "ad hoc" mathematical model, the temperature time evolution of the model surface. The temperature is measured at a distance by a thermocamera. In previous tests on delta wing models, the used thermocamera showed a limitation in the optics and did not provide an appropriate space resolution and, therefore, a detailed visualization of whole vortical structure. In the present paper this limitation has been overcome. The optics improvement has doubled the space resolution of thermocamera. Tests, made at angle of attack of 6-deg. and Mach number of 1.92, verified that this improvement was substantial. In fact, the detection of secondary vortex on delta wing model and strake vortices on a double delta wing model was made possible. Unfortunately, it was not possible to visualize details of vortical structure on a Gothic wing model. Tests showed that vortical patterns were similar to the one on delta wing model.

***Keywords*:** flow visualization, infrared thermography.

Nomenclature:

C	chord, m
c	specific heat of material, J/(kgK)
c_p	specific heat of air at constant pressure, J/(kgK)
k	thermal conductivity, W/(mK)
M	Mach number
$\dot{q}$	convective heat flux, W/m^2
Re	Reynolds number, Vc/ν
St	Stanton number, (Eq.1)
T	temperature, K
V	velocity, m/s
x	distance along the wing chord, m
y	distance along the wing span, m

Greek symbols

α	angle of attack
Δ	finite interval
δ	plate thickness, m
ε	surface emissivity
ν	kinematic viscosity of air, W/(mK)

ρ	density of air, kg/m^3
σ	Stefan-Boltzman constant, 5.67×10^{-8} W/(m^{2}K^4)
τ	observation duration time, s

Subscrits

a	ambient
aw	adiabatic wall
o	outer surface of the calorimetric plate
T	thermal
w	wall
∞	free stream

1. Introduction

It is well known that delta wing is very important in aeronautics. It provides lift and manoeuvrability at high angles of attack. Actual delta wing planforms are double delta wing and Gothic wing. The first one is employed on advanced, air superiority fighters (e.g. F-14 "TOMCAT") and next generation, High Speed Civil Transports (HSCT). The second one is employed on the current supersonic civil airplane CONCORDE and the hypersonic vehicle SPACE SHUTTLE.

The front part of double delta wing is named "strake", the back part "wing". The point of stake/wing juncture is named "kink". Strake, besides being an additional lifting surface, produces, on the lee-side, a stable vortex, persisting on the wing. This vortex energenizes the boundary layer and keeps the flow attached on the wing, at angles of attack higher than in the case of a delta wing. This enhances the airplane lift and manoeuvrability (Verhaagen, 1983; Verhaagen, 1998). On the other hand the strake vortices can generate buffet problems on the airplane tail. Knowledge of the strength and extension of these vortical structures can be useful in the airplane design.

Zuppardi (1998) already verified the capability of the Unsteady Computerized Thermographic Technique (UCTT) to be a powerful, non-intrusive diagnostic tool both for the visualization and the evaluation of the vortical structure strength on the lee-side of delta wings to be used in conjunction of other diagnostic techniques. In fact, it has been possible, by the UCTT, to obtain the surface patterns of heat flux coefficient, or of Stanton number. These patterns are the imprints of the flow field on the surface and, for the present application, of the vortical structures. Use of the thermographic technique in Aerodynamics is well consolidated. It has been already used successfully by Monti to study the boundary layer development on lifting (Monti and Zuppardi, 1987; Monti and Zuppardi, 1995) and non-lifting (Monti and Zuppardi, 1991) bodies. Monti used the UCTT to detect the laminar/turbulent transition region, separation region and so on. Carlomagno (1989) and De Luca (1995) used a thermographic technique to study Aerodynamics of delta wings in hypersonic and subsonic flows, respectively.

The UCTT evaluates the Stanton number distribution by processing the time evolution of surface temperature, measured at a distance by a thermocamera. The non-intrusivity makes the UCTT very attractive for the present application. In fact, any probe could heavily perturb the growth of vortical structures; thus the experimenter misses information. The UCTT is competitive with conventional diagnostic techniques (oil streaks, vapour screen, pressure taps, calorimetric gauges, laser Doppler velocimeter, and so on) in terms of accuracy, space resolution, easiness to use. Moreover the UCTT, providing information on the heat flux coefficient, is particularly useful in supersonic and hypersonic flows. Knowledge of heat flux, in these flow regimes, is important for the choice of the insulator coating of airplane surface.

Thermographic tests, made in (Zuppardi et al., 1998), pointed out some limitations both in the wind tunnel and in the thermographic equipment. These limitations did not allow a complete visualization of vortical structures on the models. In fact, due to the size of test chamber, it was possible to test just small models. At the same time, the optics of thermocamera did not provide a large enough space resolution.

In this paper, that is the logic continuation of Zuppardi's work, the limitations about the optics have been easily overcome thanks to an inexpensive zoom equipment. Preliminary tests on a 70-deg. delta wing model, already tested by Zuppardi, showed the benefits of improving the optics. The secondary vortex was visualized; confidence in the UCTT grew up. Tests have been made on an 80/70-deg. double delta wing, and a Gothic wing, at the maximum angle of attack (6-deg.), enabled in the wind tunnel, and at Mach number 1.92. Strake vortices on double delta wing have been visualized and the related strength evaluated. Unfortunately, this improvement in the

space resolution was not enough to visualize in details the complex vortical structure on Gothic wing. Tests on a Gothic wing showed that the vortical patterns are similar to the ones on delta wing.

2. Topology of Strake and Wing Vortices

The lee-side of delta wing, with a subsonic leading edge, is characterized by two contra-rotating vortical structures, symmetric with respect to the meridian chord (Délery, 1992; Rao and Whitehead, 1972). These vortical structures are produced by an over-pressure on the windward with respect to the lee-side.

Each vortical structure is made of three vortices inducing flow toward the lee-side. A primary vortex originates from the leading edge, if the leading edge is sharp. Flow separates along the entire leading edge length: primary separation line S_1 (Fig.1). Flow curls into the primary vortex, just inboard the leading edge, and reattaches along the primary attachment line (A_1). A secondary vortex forms beneath this vortex and is contra-rotating with respect to the primary one. Also the secondary vortex is characterized by a separation (S_2) and an attachment (A_2) line. A tertiary vortex arises beneath the secondary one and is contra-rotating with respect to this one. According to Délery, the tertiary vortex is very weak; it is practically indistinguishable.

The primary vortices induce flow toward the lee-side, producing two characteristic feather-like trails on the wing surface, symmetric with respect to the meridian chord. The induced cross flow velocity decreases toward the plane of symmetry up to disappear. Inboard the trails, the surface streamlines are attached and flow is undisturbed along straight lines from the wing apex (Rao and Whitehead, 1972). Flow field between the feather trails is 2-D. The feather pattern appears at some distance downstream the wing apex. An "apparently free vortex" region exists in the front part of the wing; no attachment line of primary vortex is detectable.

The described topology is for the vortical structures both on the strake and on the wing. It has to be expected that vortices, generated on the strake, increase in strength and extension up to the kink position. Vortices generated on the wing, increase in strength and extension from the kink up to the end. The strake vortices persist on the wing, as vortical wakes. Because of the lack of cause, driving vortices (i.e. the leading edges of the strake), it can be expected that strake vortices on the wing decrease in strength along the chord, up to bursting at some distance from the kink (Verhaagen, 1983). The vortical wake, lying on the wing, reduces the extension both of feather and of 2-D region. Figure1 sketches the described topology.

Gothic wing can be considered like a double delta wing with leading edge sweep angle and kink position changing continuously along the meridian chord. Each elementary segment of the leading edge can be considered as a strake for the following one. At each station along the meridian chord the vortex topology is made of a structure, originating from the leading edge (like the ones already described for delta and double delta wings) and a sheet of vortical wake, lying on the wing. This wake originates from each "elementary strake," upstream the station. According to Werlé (1964), who visualized the vortical structure on Gothic wing by dye filaments in a hydrodynamic tunnel, the vortical wake diverts to the leading edge. The wake spoils the feather region and mixes

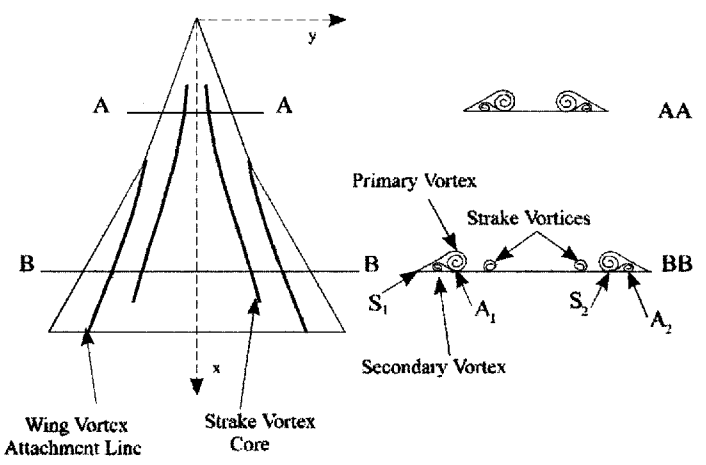

Fig. 1. Lee-side vortical structure on double delta wing.

with the primary vortex, broadening it and reducing the 2-D region.

3. Thermographic Technique in Aerodynamics

The theoretical base, allowing the use of UCTT in Aerodynamics, is the Reynolds analogy that, as well known, links the Stanton number to the skin friction coefficient. The higher the Stanton number the higher is the skin friction coefficient. No accuracy analysis of the UCTT has been made for the present tests, i.e. in supersonic flow. The UCTT has been validated successfully in subsonic flow (Monti et al., 1993). In that paper the skin friction coefficients, obtained scaling down by a Reynolds analogy the UCTT Stanton number, compare favourably with the ones measured by the Preston tube and the ones obtained processing, by the Spalding "law of the wall", the local mean boundary layer velocity, taken by a hot wire anemometer.

The Stanton number is defined as:

$$St = \frac{\dot{q}}{\rho_\infty V_\infty c_{pa} (T_w - T_{aw})} \tag{1}$$

In 2-D flow (Monti and Zuppardi, 1987), the relative minimum and maximum in the Stanton number profile identify the beginning and the end of a laminar/turbulent transition region, respectively. The beginning of the feather, on the meridian chord, coincides with a peak heating, or a relative maximum of the Stanton number profile (Rao and Whitehead, 1972). This is due to a boundary layer thinning. This point marks also the position where the beginning of the cross flow velocity, induced by primary vortices, appears. It can be assumed that along the wing centerline the boundary layer, starting from the wing apex, is removed by the induced vortex outflow; a "new" boundary layer starts on the wing meridian. The Stanton number profile will be characterized by two relative maxima. The first one is due to the above-mentioned local thinning of the boundary layer; the second one marks the end of the transition region.

In 3-D flow (Monti and Zuppardi, 1995; Monti and Zuppardi, 1991), the detection of separation regions is identified by the heuristic criterion that the convective heat flux (or the Stanton number) is larger for attached than for separated flow. As the coiled vortex, arising from a separation line, energizes the flow, the Stanton number increases up to flow reattachment; the line enveloping the maximum identifies an attachment line, i.e. the end of the separation region. The line enveloping the minimum identifies a separation line (Zuppardi et al., 1998). A relative maximum in the Stanton number profile identifies the core of the strake vortex on the wing. In fact a vortical wake on the surface increases locally the heat flux coefficient and therefore the Stanton number. In conclusions, along the semispan of strake, only a relative maximum is detectable. Along the semispan of wing two relative maxima are detectable.

For a Gothic wing it could be expected that, superimposed on the basic Stanton number profile produced by the primary vortex, a ripple due to the vortical wake should be present.

The vortex strength can be quantified by the difference between the maximum of the Stanton number and the one on the 2-D region (Zuppardi et al., 1998).

4. UCTT Mathematical Model

The unsteady 2-D heat balance equation, allowing the computation of the convective heat flux ($\dot{q}$) on the exposed surface of the model (Fig.2), and therefore of the Stanton number (Eq.1), reads:

$$\dot{q} = -\int_0^\delta \rho c \frac{\partial T}{\partial t} dz + \int_0^\delta k \left[\frac{\partial^2 T}{\partial x^2} + \frac{\partial^2 T}{\partial y^2} \right] dz - \sigma \varepsilon (T_o^4 - T_a^4) \tag{2}$$

To simplify the numerical solution of Eq.2, the physical models, used in the present tests, are made of a thin, flat plate, isotropic metallic sheet (calorimetric plate). If the calorimetric plate is thermally thin, i.e. the thickness δ is smaller than the thermal thickness δ_T, $\delta < \delta_T$:

$$\delta_T = \sqrt{\frac{k}{\rho c} \tau} \tag{3}$$

integrals in Eq.2 can be simplified:

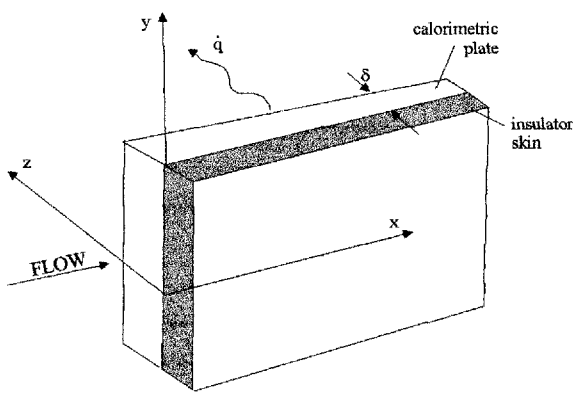

Fig. 2. Model wall co-ordinate system.

$$\int_0^{\delta} \rho c \frac{\partial T}{\partial t}\, dz \cong \rho c \delta \frac{\partial T_o}{\partial t} \tag{4.a}$$

$$\int_0^{\delta} k \left[\frac{\partial^2 T}{\partial x^2} + \frac{\partial^2 T}{\partial y^2} \right] dz \cong \delta k \left[\frac{\partial^2 T_o}{\partial x^2} + \frac{\partial^2 T_o}{\partial y^2} \right] \tag{4.b}$$

Equation 2 reads:

$$\dot{q} = -\rho c \delta \frac{\partial T_o}{\partial t} + \delta k \left[\frac{\partial^2 T_o}{\partial x^2} + \frac{\partial^2 T_o}{\partial y^2} \right] - \sigma \varepsilon \left(T_o^4 - T_a^4 \right) \tag{5}$$

Equation 5 is solved numerically by measuring the time evolution temperature. More specifically, time derivative is approximated by a forward finite difference with a first order accuracy. Two thermographic images are taken at pre-selected times t and $t + \Delta t$. The temperature in conductive terms (space derivatives) and in radiative term is approximated as the arithmetic average of temperatures at two times.

The UCTT can be implemented equivalently during either a cooling or a heating process of the model surface. The model needs to be heated or cooled (above or below the adiabatic wall temperature), before being injected into air stream.

5. Experimental Set up

5.1 Thermographic Equipment

The thermographic equipment is made of:

1. AGEMA 880 thermocamera. The thermal detector, cooled by liquid nitrogen, is HgCdTe. The sampling rate of thermal pixel is 5 μs. The optics (germanium lens 12-deg. view angle), used for the tests in (Zuppardi et al., 1998), has been supplied with a zoom equipment (12 mm extension tube). This enhanced the space resolution from 1 mm^2/pixel to 0.5 mm^2/pixel. The zoom equipment, as pointed out by remaking the calibration curve, lowered the accuracy of the temperature measurement from 0.07 K to 0.1 K.
2. A/D converter AVIORADIO DIGIMEM 64/12. This converter is able to acquire up to 11 images (i.e. 22 interlaced thermographic frames) at a pre-selected time interval (Δt), to digitalize them in a 128×128 pixels matrix, and to transfer them to a computer RAM.
3. Personal computer Pentium 100. The computer RAM stores the two thermographic images needed for the numerical implementation of the mathematical model. The equipment is supplied with a set of computer codes to: i) manage the images, ii) convert the analogic signals into temperatures by calibration curves, iii) compute the Stanton number along the chord, along the span of the wing, and the footprint on the wing surface.

5.2 Wind Tunnel

The thermographic tests have been performed in the small supersonic wind tunnel at Dipartimento di Scienza ed Ingegneria dello Spazio "Luigi G. Napolitano" (DISIS) in Naples. This is a blow-down, open test section wind tunnel. Test duration is about 10 s. The test Mach number is 1.92 and the Reynolds number per meter is 8.87×10^{7} m^{-1}. This Mach number fulfils the condition of adapted flow in the 2-D, contoured nozzle (exit section area 64×26 mm^2, length 160 mm). This condition is achieved at a stagnation pressure of 7 bar. The measured stagnation temperature, during the test, is typically 294 K, the free stream test conditions are reported in Table 1.

Table 1. Typical free stream conditions.

Density	2.09	kg/m^3
Temperature	169	K
Pressure	1.01	bar
Stream velocity	500	m/s
Adiabatic wall temperature for laminar flow	274	K
Adiabatic wall temperature for turbulent flow	280	K

5.3 Models

The sweep angle of the delta wing model (DW) is 70-deg. The sweep angles of the double-delta wing model (DDW) are 80/70-deg. The kink is located at 50% of the chord. Two parabolas, matching at 50% of the chord, define the leading edge of Gothic wing model (GW):

$$y^1 = 1.7\times10^{-3}x^2 + 0.18x$$
$$y^2 = -3.3\times10^{-3}x^2 + 0.73x - 15.3 \qquad (6)$$

The co-ordinate system of the model surface is depicted in Fig.1. The sweep angle of leading edge is 80-deg. at x = 0 and 70-deg. at x = 50% of the chord. All models are subsonic leading edge wings. In fact the normal component to the leading edge of the Mach number is: 0.66 for the DW model, 0.33/0.66 for the DDW model. For the GW model the maximum normal component of the Mach number is 0.66.

The Mach angle is 31.4-deg. The leading edges of all models are inside the Mach cone. The base span of all models is 50 mm. The wedge angle of the leading edges is 45-deg. The lengths of the meridian chord (C) are 68 mm, 92 mm and 110 mm for the DW, DDW and GW model, respectively. The planforms of the three models are shown in Fig.3. A shortcoming in using the extension tube is a loss of part of the model surface in the thermographic image. Starting from the model apex, 17 mm, 32 mm and 57 mm are lost for the DW, DDW and GW models.

The calorimetric plate of all models was a 3 mm thick sheet of brass: k = 24.9 W/m/K, ρ = 8618 kg/m^3, c = 397 J/kg/K. This thickness is able both to satisfy the thermographic requirements and to bear the aerodynamic load

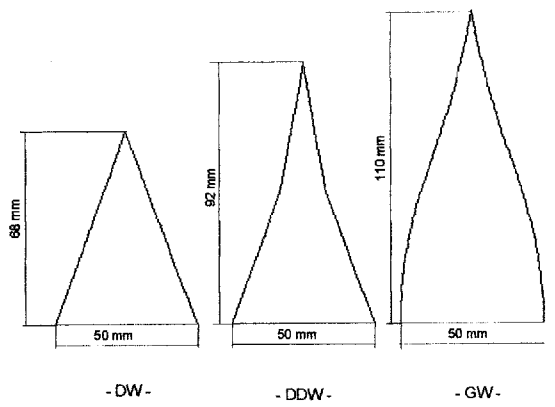

Fig. 3. Planforms of the test models: 70-deg. delta wing (DW), 80/70-deg. double delta wing (DDW) and Gothic wing (GW).

(the dynamic pressure is about 2.6×10^{5} N/m^{2}). It was assessed in (Zuppardi et al., 1998) the insulating capability of the insulating skin. The convective heat flux, computed by Eq.5, was almost two orders of magnitude higher than the conductive heat flux across the insulating skin. More specifically, it was found that the convective heat flux was 2.4×10^{4} W/m^{2} and the conductive heat flux was 5.1×10^{2} W/m^{2}.

The test surface of the calorimetric plate was blacklamp painted in order to achieve a surface emissivity close to one. The insulator skin was obtained by means of a 2 mm thick thermal insulating paste. The paste, a commercial product, is a mixture of acrylic resin, titan dioxide, glass micro-spheres and synthetic clay micro-spheres. The thermal conductivity of the paste is $k \cong 0.1$ W/m/K. The models were supplied with a self-adhesive chromen-alumel thermo-couple, located at the back surface of the calorimetric plate, i.e. beneath the insulating skin.

5.4 Experimental Procedure

For these tests the model was pre-heated. An experimental set-up has been used to inject abruptly the model into the stream. The model is previously set at a pre-selected angle of attack (all present tests were made at 6-deg.) and warmed up uniformly by a small hot air blower, at temperatures of about 325 K. This temperature was monitored by the thermocouple located at the back surface of the model. Figure 4 shows a sketch of the experimental set-up.

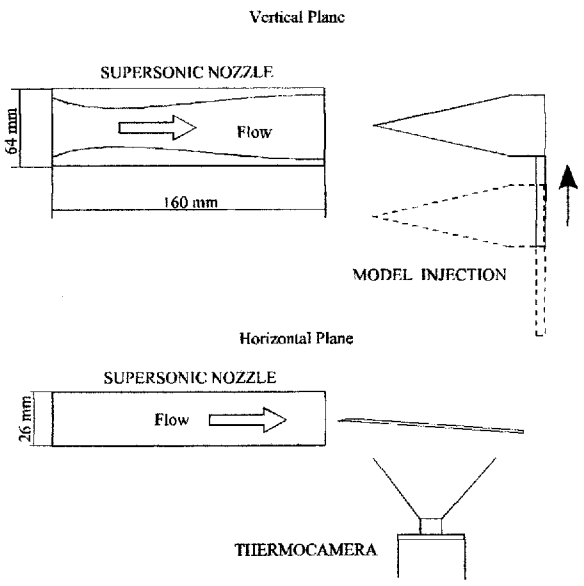

Fig. 4. Sketch of the experimental set-up.

It was found in (Zuppardi et al., 1998) that Δt = 3 s is a good compromise between the opposite requirements of improving the evaluation of the time difference temperature (that calls for a long Δt) and of improving the numerical approximation of the temperature time derivative (that calls for a short Δt). As a time of about 3 s was between the end of model heating and the model injection into the stream, and a time of about 5 s was between the model injection and the first thermographic image, the observation duration time, i.e. the cooling process time, was $\tau \cong 8$ s. Therefore $\delta_T \cong 8\times10^{-3}$ m and $\delta_T/\delta \cong 3$.

6. Analysis of Results

6.1 Delta Wing

Benefits of using the zoom equipment can be verified by Fig.5, where the Stanton number profiles, along the span of DW model, with and without zoom equipment are reported. The profile attains a minimum value at point S_1, located at the leading edge. This is a separation point, giving rise to the leading edge vortex. The increase of the profile (line S_1-A_1) indicates a reattachment process. This completes at point A_1, that is the attachment point of primary vortex. Here the profile attains an absolute maximum. The following decrease up to point B is

representative of the feather region, where cross flow velocity induced by vortex, decreases up to vanish. Flow on the region between points B-C, where the Stanton number is practically constant, has to be considered as 2-D. In (Zuppardi et al., 1998), where this model has been already tested, the secondary vortex was predicted as a relative maximum on the line S_1-A_1, i.e. point A_2. The separation point (S_2) of the second vortex is located at reattachment point of primary vortex (i.e. point A_1). As expectable strength of secondary vortex is lower than the one of primary vortex. The difference of Stanton number between points A_2-B and A_1-B are 4.0×10^{-4} and 5.3×10^{-4}, respectively.

It looks that the strength of the secondary vortex does not increase with the same rate as the primary one. In fact the secondary vortex starts to disappear at x = 54.4 mm and is not longer distinguishable on the profile at x = 63.9 mm. The secondary vortex is probably absorbed by the stronger primary vortex (see Fig.6).

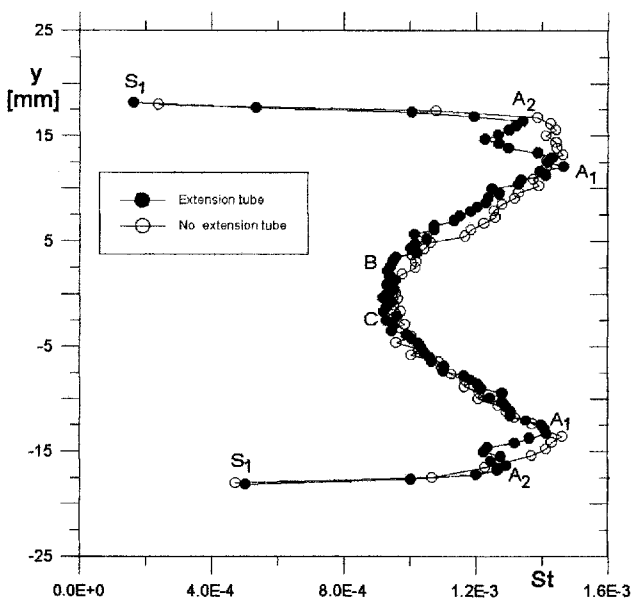

Fig. 5. Profile of the Stanton number along the span of the DW model: x= 47.6 mm, α = 6-deg., M = 1.92.

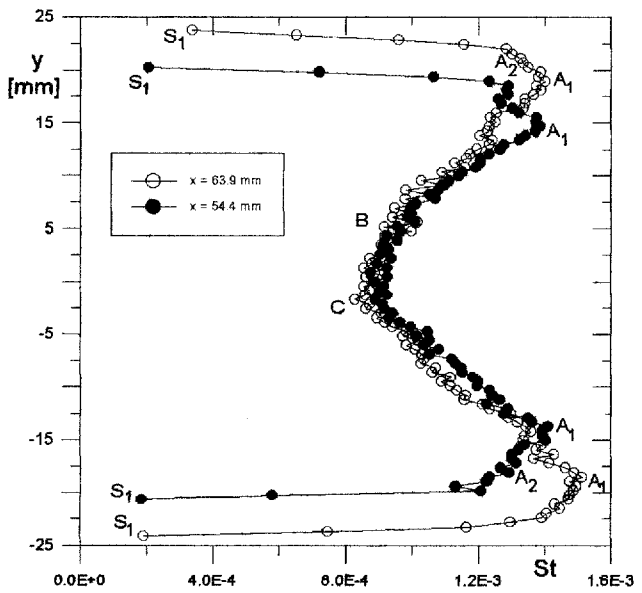

Fig. 6. Profiles of the Stanton number along the span of the DW model: α = 6-deg., M = 1.92.

6.2 Double-delta Wing

Figure 7 shows the profile of the Stanton number along three chords of DDW model: y = 0 (meridian chord), y = 3.8 mm (lying both on the strake and on the wing), y = 10 mm (lying only on the wing). The maximum on the chord at y = 10 mm indicates the vortex attachment point. Unfortunately, due to loss of model surface in the apex region, it is not possible to visualize the relative maxima, indicating the starting point of a second boundary layer on the meridian chord, and the attachment point of the vortex on the chord at y = 3.8 mm. As the sweep angle of strake (80-deg.) is higher than the one of the wing (70-deg.), the vortex strength on the wing is stronger than the one on the strake. Therefore, the perturbation of the flow stability is stronger on the wing than on the strake. This is pointed out by the laminar region extension: 16% of wing chord, 69% of strake chord. On meridian chord, where no vortex perturbation exists, the extension of laminar region is 72% of the chord.

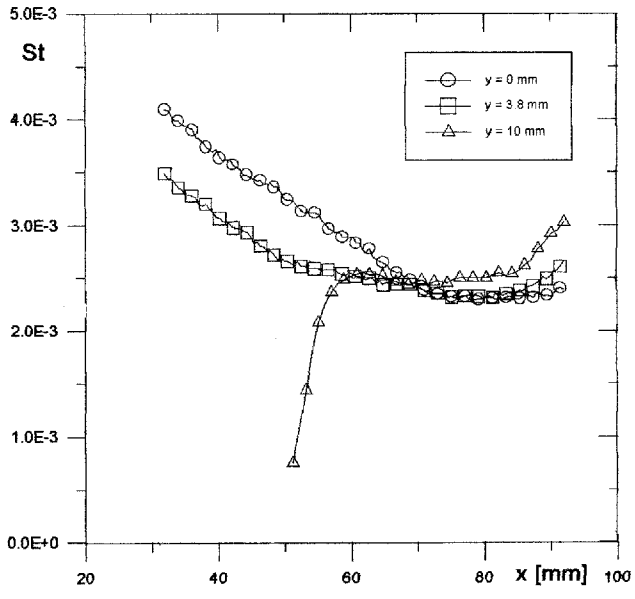

Fig. 7. Profiles of the Stanton number along three chords on the lee-side surface of the DDW model: α = 6-deg., M = 1.92.

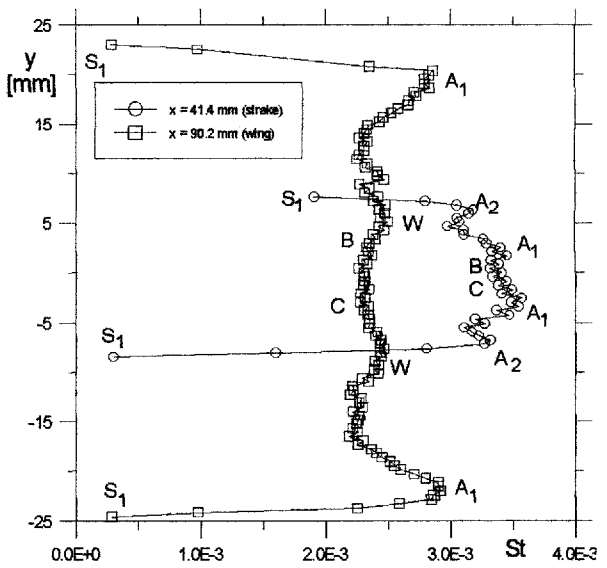

Fig. 8. Profile of the Stanton number along the span of the model DDW: α = 6-deg., M = 1.92.

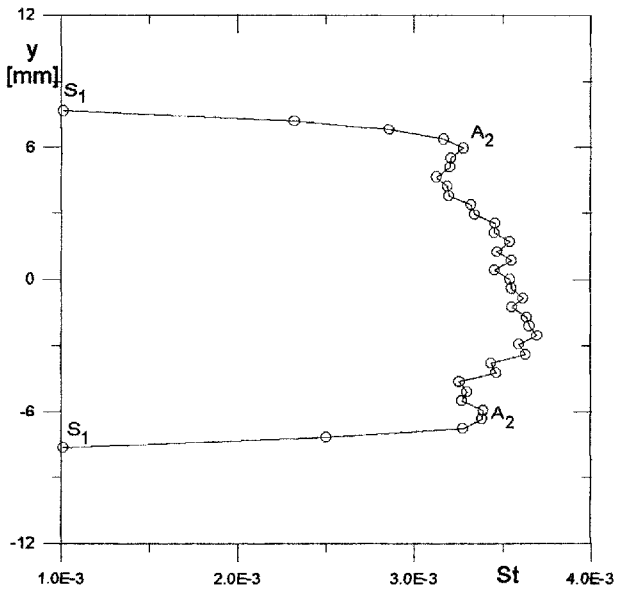

Fig. 9. Stanton number profile along the span of DDW model at x = 36.8 mm: α = 6-deg., M = 1.92.

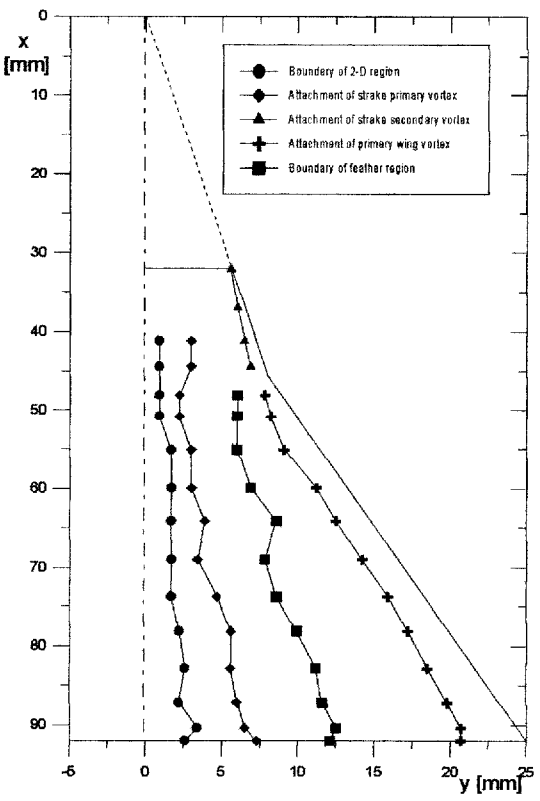

Fig. 10. Topology of vortices on DDW model: α = 6-deg., M = 1.92.

The profile of the Stanton number along the span at x = 41.4 mm (i.e. on the strake) and x = 90.2 mm (i.e. on the wing) are reported in Fig.8. As predicted, the profile on the strake shows the same vortex topology like a delta wing. The attachment point of primary vortex is marked by A_1, the one of secondary vortex by A_2. The secondary vortex at x =90.2 mm is not longer detectable on the wing. As already said, it is probably absorbed by the stronger primary vortex. The profile on the wing is modified, with respect to strake and/or to delta wing, by the presence of two relative maxima (labelled W). These are indicative of vortical wake. Region between B and C is a

2-D region. A decrease of vortex strength from the strake to the wing has to be expected. Decrease of vortex strength from the strake to the wing has to be expected. Unfortunately, due to small dimensions of the model, it is not possible to detect any decrease of strake vortex strength. The difference between the mean value of two maxima and the related 2-D value of the Stanton number is practically constant (1.96×10^{-4}) on the strake and on the wing. From the wing apex to roughly x = 36.8 mm, the wing surface is characterized by an "apparently free" vortex region (Fig.9). The primary vortices do not show any attachment point, but the secondary vortices are still detectable. In fact the relative maxima A_2 identify the reattachment point of secondary vortices. The Stanton number profile, being practically constant in the middle part of the plot, shows that the reattachment points of these vortices are not yet detectable.

Curves, enveloping the main points of the vortex topology, are drawn on the double delta wing semi-model in Fig.10. The curve labelled as "attachment of strake primary vortex" has to be understood like a vortical wake. Figure11 shows the footprint of the Stanton number.

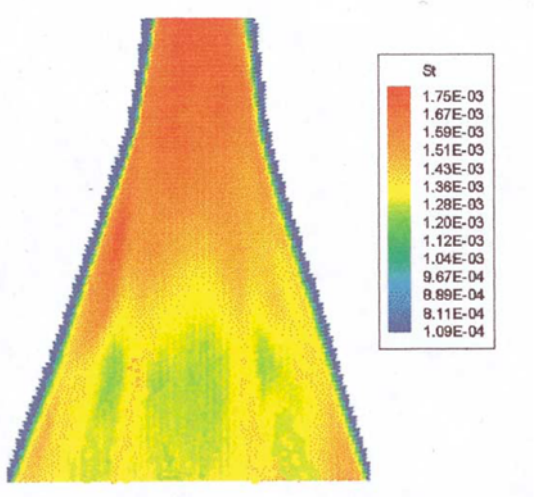

Fig. 11. Footprint of the Stanton number on DDW model: α = 6-deg., M = 1.92.

6.3 Gothic Wing

The vortex pattern on the GW model looks to be similar to the one on DW model. In fact, in the present test conditions even by zoom equipment, it was not possible to detect, on the Stanton number profile, any ripple due to the vortical sheet (Fig.12). The vortex strength on the GW model is lower than the one on the DW model; the difference of the maximum value of the Stanton number and the related 2-D value at x = 58 mm are 8×10^{-5} and

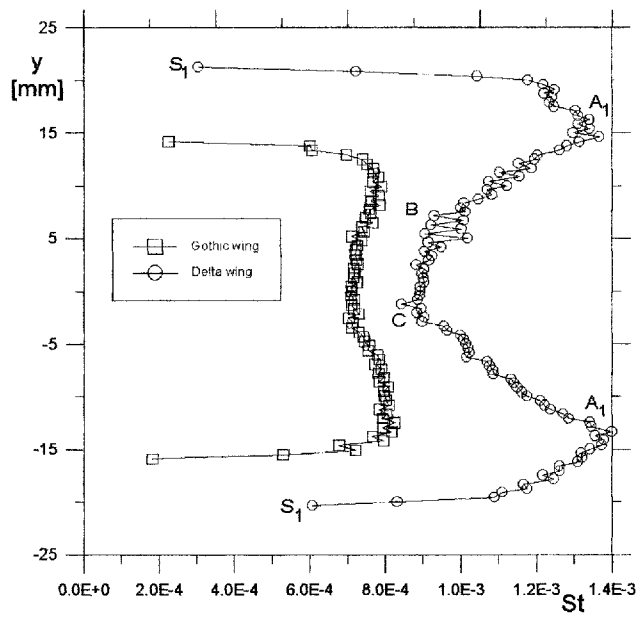

Fig. 12. Stanton number profile along the span of DW and GW model at x=58 mm: α = 6-deg., M = 1.92.

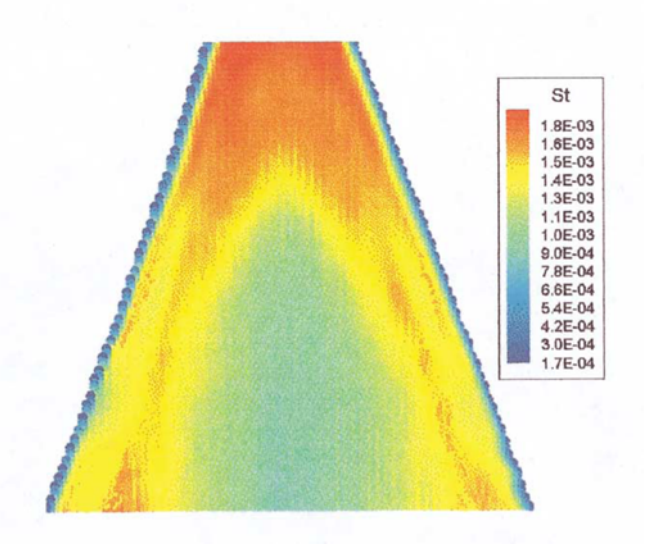

Fig. 13. Footprint of the Stanton number on DW model: α = 6-deg., M = 1.92.

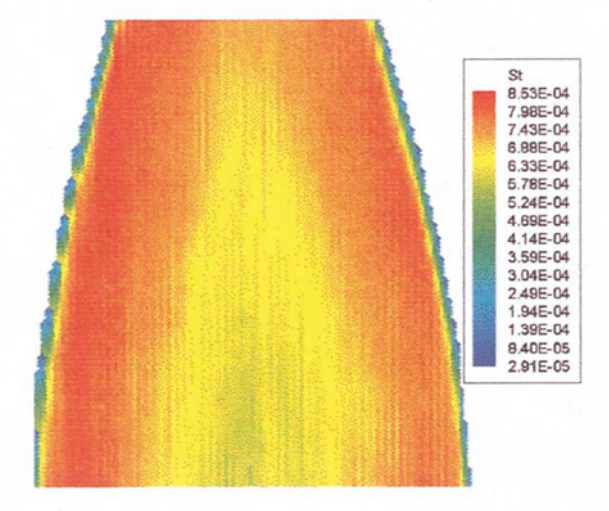

Fig. 14. Footprint of Stanton number on GW model: α = 6-deg., M = 1.92.

5×10^{-4} respectively. Correspondingly the secondary vortex strength is also very weak, therefore not detectable by the used thermocamera. This had to be expected, because the higher the sweep angle the lower is the vortex strength. The similarity of the vortex structure on GW and DW model is also supported by the comparison of the Stanton number footprints, reported in Figs.13 and 14.

7. Concluding Remarks

The Unsteady Computerized Thermographic Technique proved, once again, to be a powerful diagnostic technique in Aerodynamics. The not intrusivity makes this technique particularly suitable for the visualization of vortical structures on the lee-side surface of delta wing.

Tests have been made on a delta, double delta and Gothic wing models at angle of attack of 6-deg. and Mach number 1.92. Significant improvements were achieved in thermographic tests by enhancing space resolution of the used thermocamera by an inexpensive zoom equipment. The visualization of secondary vortex on delta wing model, of vortical wake on double delta wing model was achieved. Even though it was not possible to visualize in

details the vortical pattern on a gothic wing model, the results of the present tests encourage to going on with using more powerful thermographic equipment.

Shortcomings of UCTT are: i) test models have to be built by thin foil and need a specific pre-heating or pre-cooling technique with the related test procedure, ii) it requires an infrared optical access to the model surface.

Acknowledgments

Authors warmly thank Mr. Michele Nappi and Mr. Domenico Tavoletta for the support in experimental work.

References

Verhaagen, N.G., An Experimental Investigation of the Vortex Flow over Delta and Double-Delta Wings, Paper 7, AGARD CP-342, Rotterdam, April 1983.

Verhaagen, N.G., Tunnel Wall Effect on the Flow around a 76/40-deg. Double Delta Wing, Proceedings of the 36th Aerospace Science Meeting and Exhibit, (Reno), AIAA 98-0312, (1998-1).

Zuppardi, G., Monti, R., Russo, G.P., Evaluation of the Lee-Side Vortical Structures on Delta Wings in Supersonic Flow, Proceedings of the 8th International Symposium on Flow Visualization (8th ISFV), (Sorrento), (1998-9), 41-1 41-11.

Monti, R., Zuppardi, G., Computerized Thermographic Technique for the Detection of Boundary Layer Separation, AGARD CP N. 429 on "Aerodynamic Data Accuracy and Quality: Requirements and Capabilities in Wind Tunnel Testing" (Naples), (1987-9), 30-1 30-15.

Monti, R., Zuppardi, G., Evaluating the 3-D Effects on Finite Wings by a Computerized Thermographic technique, Atti del XIII Congresso Nazionale AIDAA (Roma), (1995-9).

Monti, R., Zuppardi, G., Detecting 3-D Turbulent Separation Regions Using Unsteady Thermographic Technique, Proceedings of the 14th International Congress on Instrumentation in Aerospace Simulation Facilities (Rockville), (1991-10), 49-59.

Carlomagno, G.M., De Luca, L., Alziary T., Heat Transfer Measurements with an Infrared Camera in Hypersonic Flow, Proceedings of the 4th International Conference on Computational Methods and Experimental Measurements (Capri), (1989-5), 467-476.

De Luca, L., Guglieri, G., Cardone, G., Carlomagno, G.M., Experimental Analysis of Surface Flow on a Delta Wing by Infrared Thermography, AIAA Journal, Vol.33, N. 8, 8-(1995), 1510-1512.

Délery, J.M., Physics of Vortical Flows, Journal of Aircraft, Vol.29, N. 5, 5-(1992), 856-876.

Rao, D. M., Whitehead, A.H., Lee-Side Vortices on Delta Wings at Hypersonic Speed, AIAA Journal, Vol. 10, N. 11, 11-(1972), 1458-1465.

Werlé, H., Fiant, C., Visualisation Hydrodynamique de L'écoulement a Basse Vitesse Autour d'une Maquette D'avion du type " CONCORDE", La Recherche Aerospatiale N. 102, 9/10-(1964), 1-19.

Monti, R., Zuppardi, G., Esposito, A., Measuring the Skin Friction Coefficient by a Computer Assisted Thermographic Technique, Proceedings of the 6th International Conference on Computational Methods and Experimental Measurements (Siena), (1993-5), 515-537.

Authors' Profiles

Gennaro Zuppardi: He received, with full score, a Laurea degree in Aeronautical Engineering in July 1976 (score: 110/110). Since Jan. 1977, he has been a fellow of the Italian Research Council. In 1981 he was promoted senior researcher in Aerodynamics at University of Naples "Federico II". He has been a lecturer in: Fluid-dynamics at the University of Basilicata in a.y. 1993/94, Experimental Fluid-dynamics at the University of Naples "Federico II" in a.y. 1994/95, Hypersonic Aerodynamics at the University of Naples "Federico II" in a.y. 1997/98.
Current mayor is:

1) Experimental Aerodynamics: i) boundary layer diagnostics by non-intrusive technique (thermography), ii) adaptive walls wind tunnel. This subject has been investigated also at NASA LaRC in a.y. 1987/88 by a fellowship of the U.S. Government.
2) Aerothermochemistry

He is author or co-author of 45 scientific papers and of a book in Hypersonic Aerodynamics.

Francesco Valenza: He received a Laurea degree in Aeronautical Engineering in Dec. 1997 (score: 107/110). Since Jan. 1998 he has been collaborating with the Dipartimento di Scienza ed Ingegneria dello Spazio "Luigi G. Napolitano" as a research assistant in experimental Aerodynamics. His major is Computerized Thermographic Technique (UCTT) and Surface Flow Visualization by Oil Technique.